STUDY OF SILICON DETECTORS FOR HIGH-RESOLUTION RADIOXENON MEASUREMENTS

Wolfgang Hennig, Christopher E. Cox, Stephen J. Asztalos, Hui Tan, Patrick J. Franz,
Peter M. Grudberg, and William K. Warburton

XIA, LLC

Sponsored by the National Nuclear Security Administration

Award No. DE-SC0004272

ABSTRACT

The radioxenon detectors currently used in applications related to nuclear explosion monitoring have a very high sensitivity to detect small amounts of radioxenon, but an improved discrimination of Xe isotopes is desirable to better distinguish the radioxenon background created by nuclear power plants and medical isotope facilities from a nuclear explosion. In the work reported here, silicon-based detectors (silicon drift detectors, PIN diodes, and Si(Li) detectors) have been explored as a possible alternative to existing systems. Silicon detectors are sensitive to X-rays, gamma rays, beta radiation, and mono-energetic conversion electrons; have very high resolution for X-ray lines that the existing systems cannot clearly separate; and as small solid state devices, can be assembled into compact systems. On the other hand, their detection efficiency is low for higher-energy photons, and available detector sizes are small, so a careful study of the improvements and drawbacks is required.

Resolutions at key energies were measured with a variety of sources and Si detectors. For example, using a small PIN diode at room temperature, we measured a full width at half maximum (FWHM) resolution of ~1 keV for 200 keV conversion electrons and 420–600 eV for 30 keV X-rays (~300 eV cooled). Detector backgrounds are extremely low, on the order of 0.005 counts/s, and practically zero if beta/photon coincidence is applied. Interactions of characteristic electrons and photons were modeled with Monte Carlo simulations to determine detection efficiencies. For electrons, the probability to deposit the full energy in an idealized Si detector is ~72% for all energies studied. For photons, it depends strongly on the energy, ranging from 86.4% at 4.1 keV to 12.0% at 30 keV and ≤ 0.6% for 80 keV and higher.

The results from measurements and simulations were used to compute the minimum detectable concentration for Xe isotopes in several possible detector geometries. We found minimum detectable concentrations of 1.5–1.9 mBq/m^3 for most isotopes with a simple 1 cm^3 cube detector with two active sides and ~0.1 mBq/m^3 for a cube with six active sides. The exception is ^{135}Xe, although the addition of a 1 inch diameter CsI detector element brings its minimum detectable concentration below 1 mBq/m^3 as well. As specifications for existing applications are 1.0 mBq/m^3, we conclude that Si detectors are indeed viable alternatives to existing detectors. Furthermore, the low background allows for fast screening of samples to determine if radioxenon is present or not, potentially useful in onsite inspections with large number of samples.

OBJECTIVES

Detection of atmospheric radioxenon is one of the tools used in nuclear explosion monitoring. Existing radioxenon detectors, e.g., the SAUNA system (Ringbom et al., 2003), the PhosWatch detector (Hennig et al., 2009) and the SPALAX system (Fontaine et al., 2004), have a very high sensitivity to detect small amounts of radioxenon. However, better determination of isotope ratios emerges as a desirable feature in future developments because this would allow a better identification of nuclear explosions in the radioxenon background from other sources like nuclear power plants and radiopharmaceutical facilities. Besides generally improving the sensitivity (i.e., lowering the background or increasing the efficiency of the detector), distinction of isotopes can also enable significant improvements by improving the detector's energy resolution so that spectral lines from the different isotopes are clearly separated in energy spectra. (In the existing detector systems, due to the low energy of the radiation and the detector materials' intrinsic resolution, key X-ray lines from different isotopes overlap.)

In recent years, progress has been made in the development of silicon-based X-ray detectors. In particular, silicon drift detectors (SDD) are now available commercially (Gatti and Rehak, 1984; Goulon et al., 2005). In this work, we therefore explored SDD, PIN diodes, and Si(Li) detectors as a possible alternative to existing detectors. Silicon detectors are not only sensitive to X-rays and low-energy gamma rays, but due to the relatively small dead layer at the detector's entrance window, they can also detect beta radiation and mono-energetic conversion electrons (CE), and they have very high resolution for the X-ray lines that the existing systems cannot clearly separate. Being small solid-state devices, they can be assembled into compact systems, and they are relatively easy to use. Potential improvements with silicon detectors in radioxenon monitoring therefore have the following features:

- Simpler cooling requirements than HPGe (can use Peltier elements or even operate at room temperature)
- Improved energy resolution for K X-ray lines
- Ability to use additional L X-ray lines in radioxenon detection, including L-K and L-beta coincidences
- Improved energy resolution of mono-energetic conversion electrons
- Ability to detect ^{37}Ar, which only emits L X-rays, in the same detector
- No expected memory effect, being a metal (oxide)
- Low background due to less-massive detector; no lead shielding required
- Ability to add a permanent calibration source, e.g., ^{55}Fe at 5.9 keV (no overlap with Xe lines)

On the other hand, their detection efficiency is low for higher-energy photons, and available detector sizes are small, so that a careful study of the improvements and drawbacks is required. We therefore had the following three objectives in this project:

1. Simulate radiation interactions in Si detectors
2. Measure resolutions and backgrounds with Si detectors and test sources
3. Use results to estimate sensitivity to radioxenon

Where appropriate, results are compared to the published performance of existing detectors, in particular the beta/gamma coincidence systems SAUNA and PhosWatch.

RESEARCH ACCOMPLISHED

Application Background Information

The four Xe isotopes of interest in radioxenon monitoring, listed in Table 1, all emit one or more beta particles or CE simultaneously with one or more gamma rays or X-rays. In the existing detector systems, beta-gamma coincidence is therefore often used to suppress the detector's natural background rate, using a dedicated detector or detector layer for each type of radiation. The Si detectors can detect both types, so two identical detectors can be used for coincidence detection; furthermore, they can also detect L X-rays, which are not detected in any of the existing systems due to their low energy.

Table 1. Xe isotopes used for nuclear monitoring and their characteristic radiations in keV and abundance (abd) in percent (Browne and Firestone, 1986). In the final column, ^{37}Ar is shown for reference. The metastable isotopes ^{131m}Xe and ^{133m}Xe decay to a Xe ground state and emit Xe X-rays; the other isotopes emit Cs X-rays

Isotope	^{135g}Xe		^{131m}Xe		^{133m}Xe		^{133g}Xe		^{37}Ar	
Half life	9.1 hours		11.9 days		2.19 days		5.25 days		35 days	
	E keV	abd	E keV	abd	E keV	abd	E keV	abd	E keV	abd
L X-rays	4.3	0.28	4.1	3.6	4.1	3.3	4.3	2.5	2.6	8.2
	4.7	0.25	4.5	3.0	4.5	2.9	4.7	2.3	2.8	0.5
K X-rays	30.6	1.5	29.4	15.5	29.4	16.2	30.6	14.1	--	
	31.0	2.8	29.8	28.9	29.8	30.1	31.0	26.0		
	35.0	0.76	33.6	7.8	33.6	8.1	35.0	7.1		
	36.0	0.29	34.6	1.9	34.6	1.9	36.0	1.7		
Gamma rays	250.0	90	163.9	2.0	233.2	10.3	81.0	37.0	--	
Beta particles	< 905	97	--		--		< 346	99	--	<0.3
Conversion electrons (CE)	214	5.7	129	60.7	199	63.1	45	54.1	--	
	244	0.8	158	14.0	228	21.0	75	6.6		
			159	15.1	232	4.7	76	1.7		
			163	6.7	233	1.2	80	1.7		
			164	1.6						

Simulations to Determine Interaction Probabilities

The main motivation for performing Monte Carlo simulations on silicon detectors was to obtain data to compute their coincidence detection efficiency for photon/electron pairs generated by the radioactive xenon decay. Key photon and electron energies from 4.1 to 905 keV were simulated with PENELOPE-2008. Figure 1 shows the geometry of the simulated detector. Xenon gas with a volume of 1 cm^3 is enclosed in a cube surrounded by two 100 mm^2 area, 450 µm thick windowless SDD at the top and bottom as well as four 0.5 mm thick stainless steel side walls. (The term "windowless" means that there is no encapsulation or other external barrier between the silicon and the gas, only the intrinsic dead-layer of the silicon itself.) Two 1 inch CsI cylindrical crystals were placed behind two parallel stainless steel side walls. The Si detector was assumed to have a 0.1 µm thick dead layer and a 2 mm silicon substrate layer behind the active volume. The assumed thickness of the Si detector matches commonly available devices; thicker detectors would increase the detection efficiency but become difficult to manufacture in good quality. This geometry provides information for a number of possible detector geometries by simple extrapolation of the results. For example, for a basic detector with only two active Si detector sides, the CsI interactions can simply be ignored. For a six-sided detector, equivalent interactions in four additional sides can be added by symmetry (there are no directional preferences in the Xe decays). We assumed a point source at the center of the Xenon gas volume emitting radiation isotropically. A total of 100,000 radiation events were generated for each photon or electron energy. Energies deposited in each detector component were recorded and used to generate energy histograms and to compute interaction probabilities. These interaction probabilities include the geometrical solid angle factor, e.g., of the 100,000 radiation events starting at the center of the xenon gas cell, only one-sixth of the events would initially travel towards one silicon detector, so the maximum interaction probability per silicon detector is 16.7%. Coincidence detection efficiencies can then be computed as products of interaction probabilities.

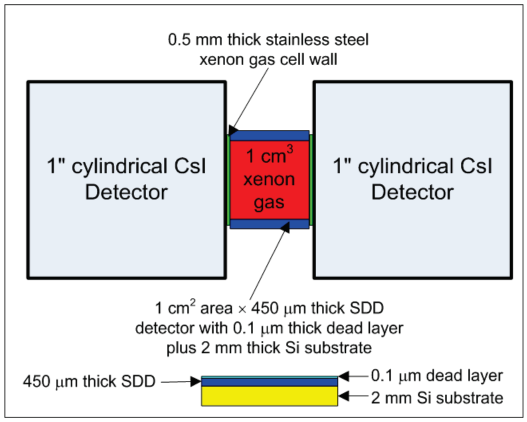

Figure 1. Drawing of the simulated Xe silicon detector geometry.

Table 2 shows interaction probabilities for several simulated radiations. "Full energy" deposited in a detector means the deposited energy is within a typical FWHM resolution of the source energy, so the event will fall into the peak region of interest (ROI) in the spectrum. The number shown is the average of both detectors. For electrons, the full-energy deposition probability is typically about 12% per Si detector side (compared to a maximum 16.7% due to geometry) and is essentially zero in the secondary CsI detectors outside the cell. For photons, the full energy deposition probability depends strongly on the energy, ranging from 14.4% to 0% for the Si detector and 0% to 21% for the CsI detector as energies increase from 4.1 keV to 250 keV.

Table 2. Full energy deposition probabilities for simulated radiations. Very small or irrelevant numbers are omitted. For CsI, numbers for electron interactions in parentheses are the probability of depositing any, not full energy.

	Fully stopped in xenon gas	Full energy deposition in dead layer of one SDD	Full energy deposition in one SDD (geometric max. 16.7%)	Full photon energy deposition in one CsI (any electron energy)	Full energy deposition in all stainless steel walls	Not inter-acting	Other iterations (e.g., substrate)
4.1 keV X-ray	11.5%	0.1%	14.4%	0%	58.4%		1.1%
31 keV X-ray			2.0%	4.0%[1)]	65.7%		22.3%
81 keV γ			0.1%	21.2%	12.2%	36.0%	9.4%
164 keV γ				21.1%	1.5%	48.5%	7.8%
250 keV γ				14.6%		61.2%	9.7%
45 keV CE			12.4%	(0%)			
129 keV CE			12.2%	(0.05%)			
199 keV CE			12.4%	(0.12%)			
346 keV β endp.			12.1%	(0.34%)			
905 keV β endp.			0.7%[2)]	(2.13%)			

Notes
(1) Stainless steel blocks a large fraction of low-energy X-rays. Al or Be walls would be better.
(2) A large fraction of the 905 keV electrons pass through the Si detector, depositing some energy but not the full 905 keV. Since in Xe measurements 905 keV is only the end point of the beta distribution, there is no "beta peak" in any case, and we can still assume that roughly 12% of high-energy betas deposit a measurable amount of energy in the SDD and are counted in the coincidence ROI (E_β ~10 … 905 keV).

The total interaction probability of electrons with one silicon detector (depositing any amount of energy) was about 22% to 24% for all electron source energies, which is greater than the probability of one-sixth (16.7%) determined by the simple geometric solid angle. This is caused by the fact that electrons can backscatter when interacting with the silicon detector parts and deposit energy in both Si detectors.

Experiments to Study Electron Response in Si

Initial studies with a Si(Li) detector focused on the electron response as a function of energy and window thickness (Figure 2). Si(Li) detectors are operated at 77K and thus are not desirable for radioxenon monitoring applications, but as the dead-layer thicknesses in the front entrance windows of Si(Li), PIN or SDD detectors are approximately the same (about 0.1µm), the response to electrons is similar for all three types of Si detector. For the measurements presented in Figure 2, the detector was encapsulated and cooled in a vacuum insulated cryostat with a thin polymer vacuum-tight window. Two source configurations were used. In the first, the source was positioned in air outside the cryostat at varying distances from the detector's polymer window. In the second, windowless, configuration, the source was mounted close to the Si(Li) crystal inside the cryostat vacuum, so there was no absorbing material between the source and the Si(Li) crystal. The ^{109}Cd isotope was coated onto the end of a small needle with no encapsulation, thus permitting electrons to be emitted with minimal attenuation. The energy resolution of ^{109}Cd conversion electrons at 63 and 85 keV is seen to degrade as a function of source-to-detector distance, and the centroids shift to lower energies. The windowless configuration shows the least degradation and shift. This behavior is readily understood in terms of electron straggling in the air gap and the thin polymer window. These measurements suggest that the ideal detection arrangement should involve a windowless detector and a minimal source-to-detector gap.

Additional tests were performed to study the minimum electron energy detectable by a Si detector, as the intrinsic dead layer in the Si crystal stops very low energy electrons. Contributions from 5 keV Auger electrons were visible in the energy spectra of windowless detectors, though no clear peak was formed. We conclude that such low-energy electrons are not useful for quantitative analysis—quite unfortunately, since Xe isotopes also emit a large number of these Auger electrons—and that the minimum useful electron energy is around 10–20 keV. This is consistent with a thickness of the dead layer of ~0.1 µm, a well-established published number in the literature.

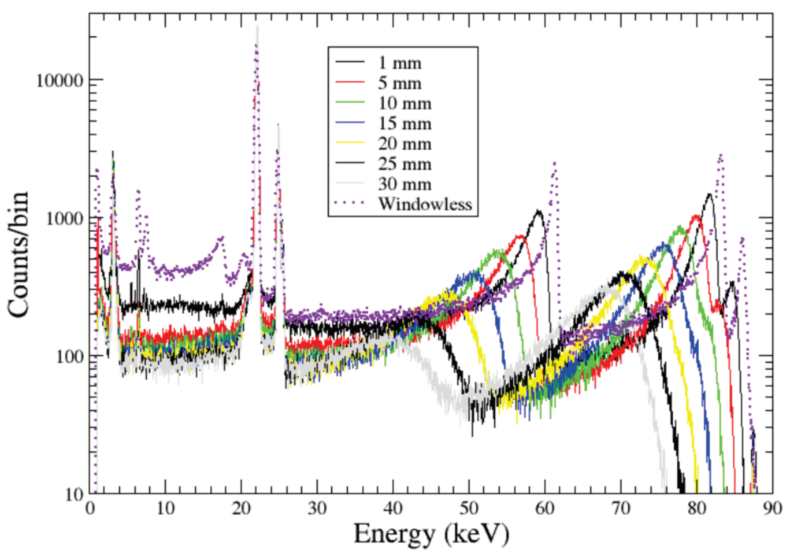

Figure 2. The electron response as a function of air gap for a PGT Si(Li) detector using a ^{109}Cd needle source. In the case of the windowless configuration, the source was mounted inside the Si(Li) cryostat vacuum, so the air gap was effectively zero.

Experiments to Compare SDD and PIN Diodes

For the purpose of radioxenon monitoring, the only practical detectors are those that do not require liquid nitrogen cooling, i.e., PIN diodes and SDDs. Generally, PIN diodes are cheaper than SDDs; and when cooled to moderate temperatures (-20 C to -40 C) small PIN diodes and SDDs can achieve similar resolution. However, higher temperatures and larger PIN sizes, the effects of leakage currents and capacitance worsen the resolution of PIN diodes. In contrast, even large SDDs have relatively low capacitance and low leakage currents and therefore maintain good resolution at higher temperature. Although both PIN and SDDs have easy-to-use cooling options with built-in Peltier coolers, it may be desirable to dispense with cooling to simplify operation, especially to alleviate concerns associated with water condensation on windowless detectors. In this case, SDDs theoretically offer a resolution advantage over PIN diodes for the reasons stated.

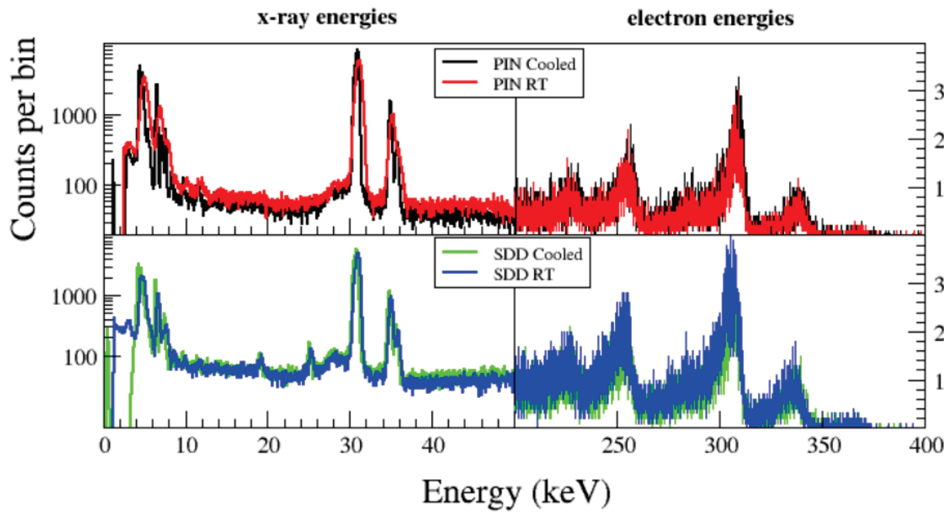

Figure 3. Bottom row: X-ray (left) and electron (right) response for the 7 mm^2 SDD cooled and at room temperature (RT) using a ^{133}Ba disk source. Top row: Same, but for the 6 mm^2 PIN diode.

A key criterion for use in radioxenon monitoring applications is that the Si detector should be able to resolve the ~30 keV Xe K_α X-rays emitted by ^{133m}Xe and ^{131m}Xe from the ~31 keV Cs K_α X-rays emitted by ^{135}Xe and ^{133}Xe while also providing adequate resolution and dynamic range for betas and CEs. Consequently, the response of SDD and PIN diode detectors to electrons and photons was explored while cooled and at room temperature (RT).

The electron and photon response of a 7 mm^2 × 0.45 mm SDD (Amptek XR100-SDD) versus that of a 6 mm^2 × 0.5 mm PIN diode (Amptek XR-100CR), both with a 25 μm Be window detector, are shown in Figure 3. Measurements were made with the detectors at RT and cooled. A ^{133}Ba source was used as a surrogate for decay products from the Xe isotopes. Neither the electron nor the X-ray performance of the SDD or the small PIN diode is degraded significantly at RT. The PIN diode is seen to have slightly poorer overall response than the SDD, and RT operation is slightly poorer than cooled operation. However, even at RT the small PIN diode has sufficient resolution (~0.4 keV @ 30 keV) to resolve the 30/31 keV X-rays.

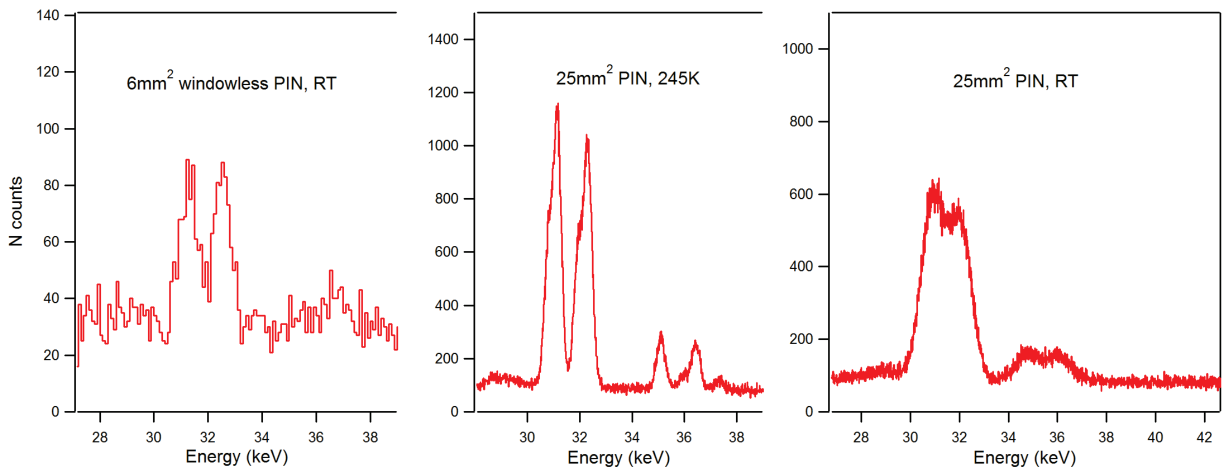

Figure 4. X-ray lines of PIN diodes from ^{137}Cs and ^{133}Ba. The separation of these two lines closely approximates that expected from the decay of ^{133m}Xe or ^{131m}Xe vs ^{133}Xe or ^{135}Xe.

Figure 4 shows spectra from mixed ^{133}Ba and ^{137}Cs sources to illustrate this further. A windowless 6 mm^2 × 0.5 mm PIN diode detector was clearly able to resolve the 30.9 keV K_α X-ray from the decay of ^{133}Ba from the 32.1 keV K_α X-ray from the decay of ^{137}Cs. A cooled 25 mm^2 PIN diode was able to do likewise, but if it is operated close to RT, the resolution worsens so that the peaks begin to overlap. This particular PIN diode, however, is old and not quite state-of-the-art design; newer large PIN diodes can be expected to have better resolution.

Measurements of Energy Resolutions and Backgrounds

In further tests, a 6 mm^2 windowless PIN diode was used for measurements of energy resolution and backgrounds. Key resolutions are listed in Table 3. Figure 5 presents X-ray and electron energy spectra using windowless sources of ^{109}Cd, ^{133}Ba, and ^{137}Cs and an air gap of ~1 mm to the detector. Figure 6 shows the energy spectrum acquired with the windowless PIN in Xe measurements at the University of Texas at Austin, where a mixture of ^{133m}Xe and ^{133}Xe was obtained by irradiating stable ^{132}Xe.

In the Xe measurements, the acquisition was broken into two 2 h runs with different peaking times (Tp) to optimize energy resolution for different energy ranges. The spectra show peaks for the 30 and 31 keV X-rays from ^{133m}Xe and ^{133}Xe, respectively, for the 45 keV CE from ^{133}Xe, and for the 199 and 229 keV CEs from ^{133m}Xe. Also visible are the ~35 keV X-rays (K_β). Resolutions are 564 and 618 eV FWHM for the X-rays and 1.0–1.3 keV FWHM for the high-energy CEs.

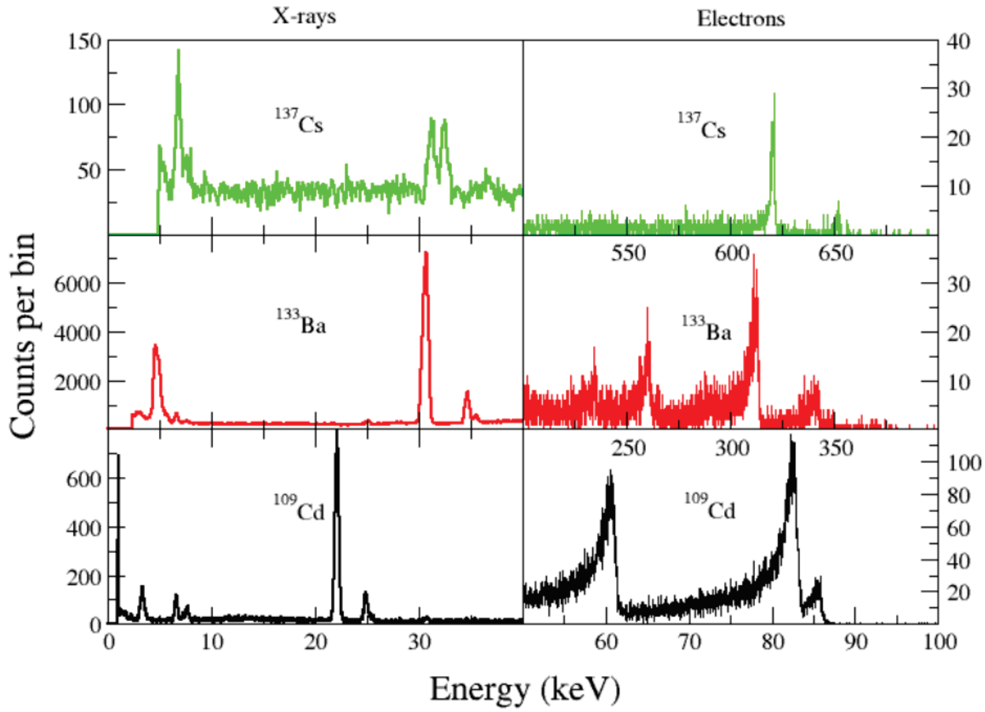

Figure 5. The X-ray and electron response of the windowless PIN diode using ^{109}Cd, ^{133}Ba, and ^{137}Cs open needle sources. Though the X-ray response is undifferentiated from that of the windowed PIN diode (Figure 3), the electron response of the windowless PIN diode is significantly improved. Note that X-ray lines well below 5 keV are visible in the ^{109}Cd spectrum, indicating ^{37}Ar is also detectable by this detector.

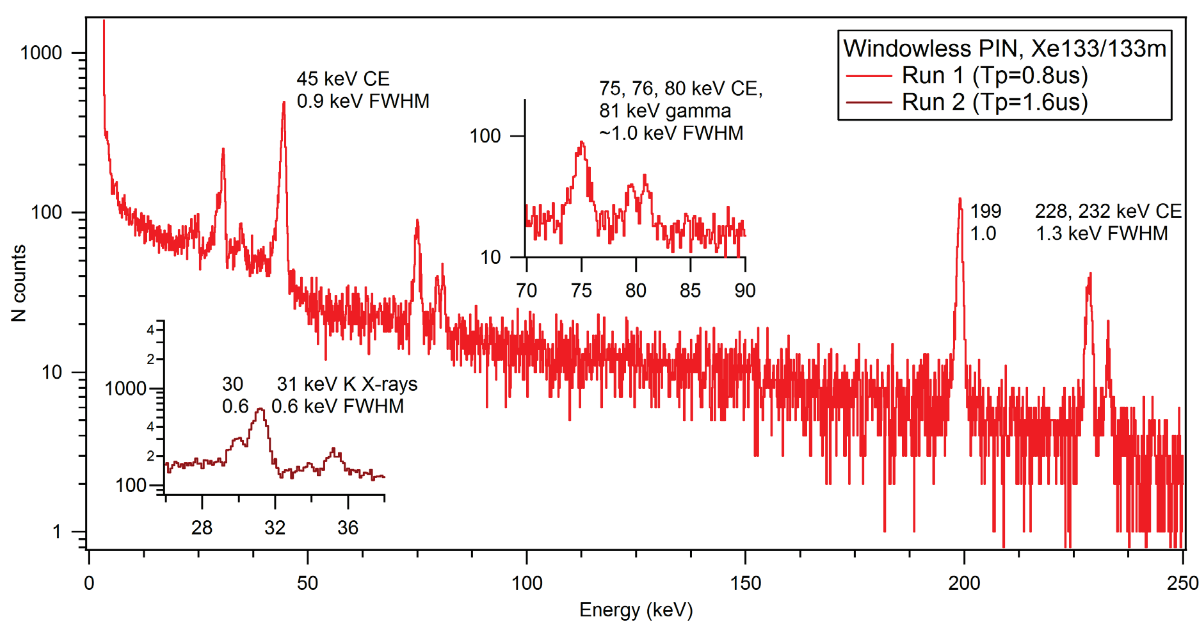

Figure 6. The X-ray and electron response of the windowless PIN diode for a mixture of ^{133}Xe and ^{133m}Xe.

Figure 7 shows data from a background measurement with a 50 mm^2 SDD, acquired for 3.9 days. This demonstrates that besides improved resolution, the extraordinarily low background rates in the Si detectors (SDD or PIN) is another main attribute distinguishing them from existing radioxenon detectors. As there are no clear features in the background spectrum, for the sensitivity calculations below, we assume the counts to be evenly distributed with energy, for a total of B_{full} = 0.0054 counts/s over the full range of R_{full} = 0–800 keV for a 100 mm^2 Si detector.

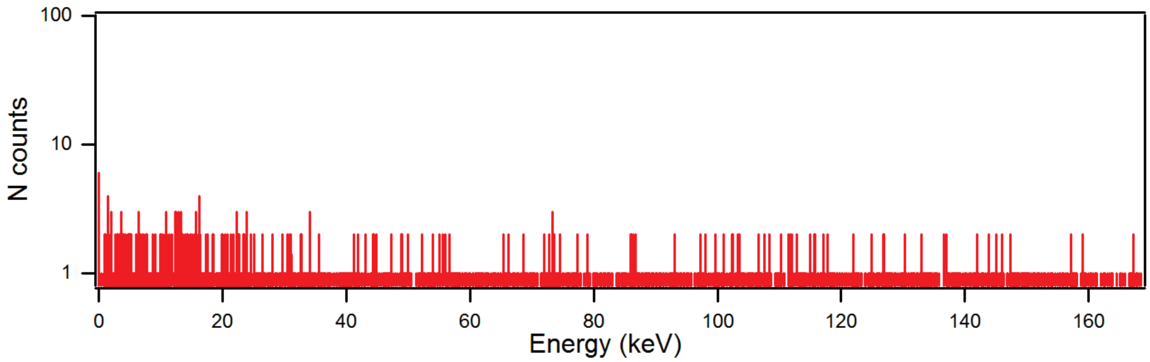

Figure 7. Background spectrum from a 50 mm^2 SDD, 3.9 days.

Table 3. Energy resolutions from PIN diodes. As described above, SDD resolutions are comparable to small PIN diodes or cooled large PIN diodes, even for large SDDs. Note that even the windowless detector is operated with an air gap of ~1 mm for solid sources, causing broadening and shift of the CE peaks which are not present in the Xe measurements. Variations in resolutions at nearby X-ray energies come from the structure of the underlying doublets. Resolutions of existing beta/gamma detectors are typically ~30% for 30 keV X-rays (~10 keV) and ~30% for most CEs (e.g., ~60 keV at 199 keV).

Energy (keV)	FWHM Resolution (keV)	Type	Source	Detector	Temperature
3.0	0.188	X-ray	Cd109	PIN, 6mm^2	RT
5.9	0.330	X-ray	Fe55	PIN, 6mm^2	RT
5.9	0.161	X-ray	Fe55	PIN, 6mm^2	cold
22	0.440	X-ray	Cd109	PIN, 6mm^2	RT
25	0.261	X-ray	Cd109	PIN, 6mm^2	cold
30	0.564	X-ray	Xe133m	w/l PIN, 6mm^2	RT
31	0.618	X-ray	Xe133	w/l PIN, 6mm^2	RT
31	0.636	X-ray	Ba133	w/l PIN, 6mm^2	RT
31	0.582	X-ray	Ba133	PIN, 25 mm^2	cold
35	0.450	X-ray	Ba133	w/l PIN, 6mm^2	RT
35	0.315	X-ray	Ba133	PIN, 6mm^2	cold
45	0.852	CE	Xe133	w/l PIN, 6mm^2	RT
81	1.456	gamma	Xe133	w/l PIN, 6mm^2	RT
81	0.584	gamma	Ba133	w/l PIN, 6mm^2	RT
88	0.536	gamma	Cd109	PIN, 6mm^2	RT
199	1.098	CE	Xe133m	w/l PIN, 6mm^2	RT
229	1.319	CE	Xe133m	w/l PIN, 6mm^2	RT
266	2.546	CE	Ba133	w/l PIN, 6mm^2	RT
348	7.651	CE	Ba133	w/l PIN, 6mm^2	RT
656	1.538	CE	Cs137	w/l PIN, 6mm^2	RT

Coincidence Measurements

Further measurements were made with two detectors to extract coincidence events. Figure 8 shows ^{133}Ba coincidence spectra between an SDD and the windowless PIN diode. The ^{133}Ba creates ~4, 30, and 35 keV X-rays, 80 keV and higher gamma-rays, and CEs between 200 to 350 keV. The X-rays detected in one detector are in coincidence with CEs (outside the energy range shown in the figure) and Compton scattered gamma rays detected in the other detector. The deposited energy for the Compton interaction varies while the energy from the X-rays is fixed, so the coincidence events form horizontal and vertical lines.

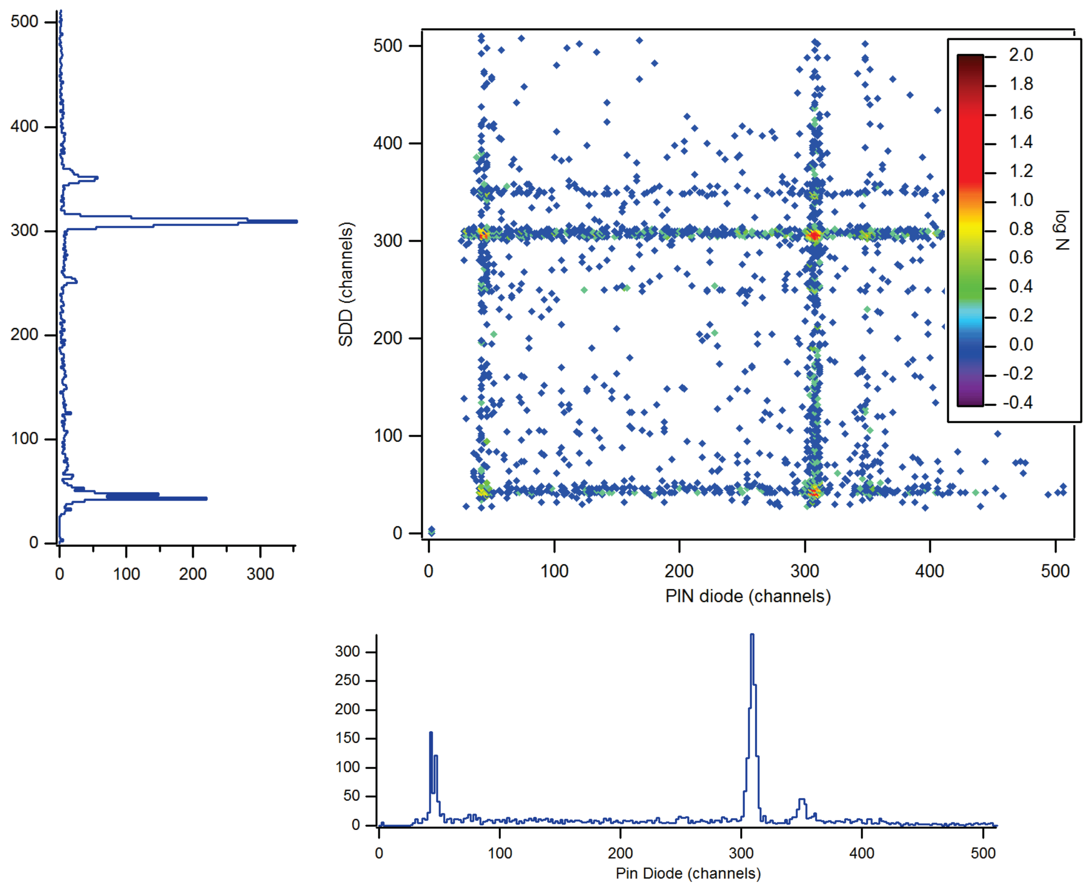

Figure 8. The ^{133}Ba coincidence spectrum (energy range ~50 keV) from the windowless PIN diode and a 7 mm^2 SDD. Note that coincidences with L X-rays are also detected.

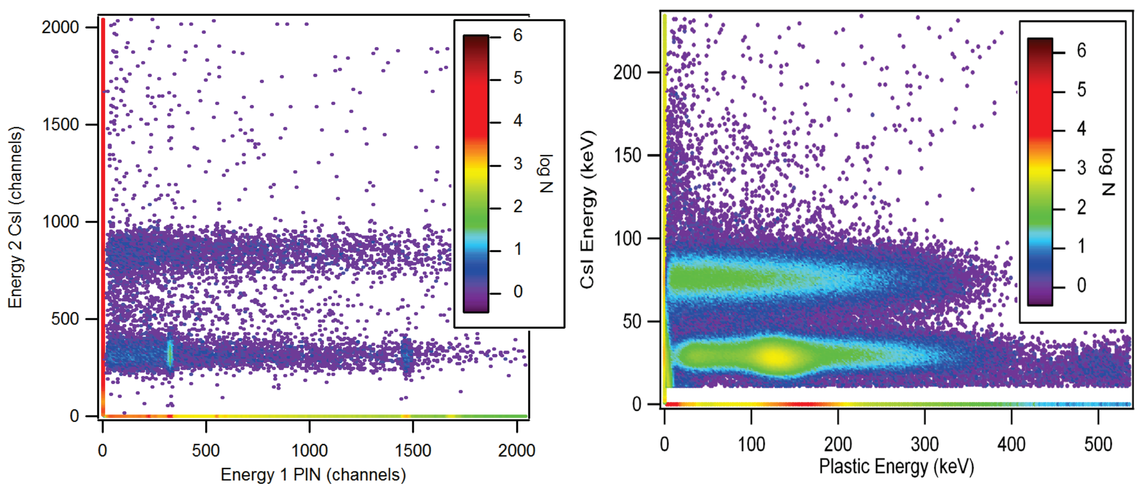

Figure 9. (left) PIN-CsI coincidence spectrum for a mixture of ^{133}Xe and ^{133m}Xe. The energy range of the x-axis is ~200 keV. (right) PhosWatch plastic-CsI coincidence spectrum for a mixture of ^{133}Xe and ^{131m}Xe (from Hennig et al., 2007). The projection of the PIN-CsI data to the horizontal axis is identical to Figure 6.

Since our gas cell for Xe measurements accommodated only one Si detector, coincidence measurements with Xe were performed using the windowless 6 mm^2 PIN and a 1 inch CsI crystal outside the cell (Figure 9, left). The CsI does not detect betas or CEs, so there are no coincidences with X-rays detected by the PIN. From the photons detected by the CsI, we see two broad lines at 30/31 and 80 keV, forming bands of coincident events with betas/CEs detected by the PIN. The CE coincidences form two clear peaks within the 30/31 keV band: 31 keV X-rays in the CsI in coincidence with 45 keV CE in the PIN (from ^{133}Xe, at PIN channel ~300) and 30 keV X-rays in the CsI in coincidence with 199 keV CE in the PIN (from ^{133m}Xe, at PIN channel ~1400). With two Si detectors inside the Xe cell, both axes would include beta lines and high-resolution X-ray and CE peaks; beta/X-ray and CE/X-ray coincidences would be separated by the X-ray energy difference. In contrast, a typical coincidence spectrum from a PhosWatch, one type of the existing beta/gamma detectors, has much poorer resolution (Figure 9, right).

Estimate of Sensitivity

To estimate the sensitivity of silicon detectors for radioxenon monitoring, we studied three detector geometries:

A. A 1 cm^3 cube Si detector with two active sides, 100 mm^2 active area each. This geometry has two coincidence permutations (beta left, photon right, and vice versa).

B. A 1 cm^3 cube Si detector with six active sides, 100 mm^2 active area each. This geometry has 30 coincidence permutations (beta in side 1 … 6, photon in any other, and vice versa).

C. A 1 cm^3 cube with a 100 mm^2 Si detector on one side and a 1 inch CsI crystal on a second. This geometry has one coincidence permutation (beta Si, photon CsI)

In radioxenon monitoring, sensitivity is usually expressed as the minimum detectable concentration (MDC). Starting with the MDC definition described by Anderson and Ringbom (2003), we can simplify the equations by disregarding decays during collection, processing, and measurement of the radioxenon and arrive at

$$MDC = n_{LD} / (\varepsilon_{\beta\gamma} * \beta\gamma * t_{acq} * V)$$
$$n_{LD} = 2.71 + 4.65\ \sigma$$
$$L_c = 2.33\ \sigma$$
$$\sigma^2 = D_n\ ,$$

where D_n is the measured background counts in region of interest (ROI) n, $\varepsilon_{\beta\gamma}$ is the coincidence detection efficiency for the ROI, $\beta\gamma$ is the branching ration into the ROI, V is the collected air volume, and t_{acq} is the measurement time, assumed to be 24 h. The numericals for L_c and n_{LD}, critical limit and detection limit, come from the classic paper by Currie (1968).

The efficiency $\varepsilon_{\beta\gamma}$ is computed from our simulations described above. As an example, consider ^{131m}Xe: In geometry A, coincidences between 30 keV photons and 129 keV CEs have a 2.0% photon interaction probability, 12.2% CE interaction probability, and two coincidence permutations. The efficiency is the product of these numbers, resulting in $\varepsilon_{\beta\gamma\text{-}30\text{-}129}$ = 4.88E-3. The branching ratio $\beta\gamma_{30\text{-}129}$ = 54% is obtained from literature. A second coincidence branch involves ~4 keV L X-rays and 159 keV CEs, with $\varepsilon_{\beta\gamma\text{-}4\text{-}159}$ = 3.54E-2 and $\beta\gamma_{4\text{-}159}$ = 6.6%. For such multiple branch isotopes, the term ($\varepsilon_{\beta\gamma}$* $\beta\gamma$) in the above equation is replaced by the sum of these products.

The background D_n in the coincidence ROI is the product of (1) the background rates in each detector, (2) a 100 ns coincidence window, (3) the measurement time, and (4) the number N_{cp} of coincidence permutations. ROI background rates are derived from the measured, full energy range background rates B_{full} by scaling them with the width and height of the ROI, so that overall

$$D_n = B_{full}^2 * 10^{-7}s * N_{cp} * t_{acq} * (ROI_n\ width * ROI_n\ height / R_{full}^2).$$

ROI width and height are set by the energy resolution for the ROI energy, typically 2× FWHM. For isotopes with multiple ROIs, σ^2 is the sum of the D_n counts in all these ROIs. In the case of Si detectors, the ROI background counts are well below 1, so the term 2.71 dominates n_{LD}. Background contributions from other isotopes and previous measurements do not occur because ROIs do not overlap and Si is assumed to have no memory effect.

The air volume V is given by the Xe collection system, which is independent of the detector. For the calculations below, we start with the assumption of typical values of ~20 m^3 in radioxenon monitoring stations, resulting in ~2.3 cm^3 of stable Xe. However, as detector geometries A–C only have ~1 cm^3 active volume, compared to ~5 cm^3 in a PhosWatch (and similarly SAUNA) detector, we adjust V by a factor equivalent to the ratio of active volumes and use V = 4 m^3.

For our calculations, it does not matter if the Si detector is an SDD or a PIN diode, as long as the resolution is sufficient to separate the 30 and 31 keV X-ray lines. For simplicity, we ignore effects from multiple electron interactions from backscatter processes and the triple coincidences in ^{133}Xe. With these assumptions and simplifications, we believe our MDC estimates to be reasonably accurate, to within maybe a factor of 2 to 5. For comparison, we also will list MDCs reported for existing detectors. These quoted values do not include the above simplifications, and test conditions may vary from our assumptions.

Table 4 lists the efficiency and the background in the 30/31 keV ROIs as examples of the calculations, then the end result of n_{LD} and MDC for all ROIs combined. Also shown is the Xe concentration corresponding to one count and the net counts with error for 10 mBq/m^3 of each Xe isotope.

Table 4: MDC, n_{LD} for radioxenon isotopes (values for SAUNA from Gohla and Auer, 2010)

Detector	Isotope	$\varepsilon_{\beta\gamma\text{-}30}$	D_{30}	Total n_{LD}	Total MDC	1 net count in ROIs corresponds to	Net counts for 10 mBq/m^3; error (%)
A (2 sides)	^{131m}Xe	4.88E-3	3.54E-11	2.71	1.58 mBq/m^3	0.58 mBq/m^3	17 +/- 24%
B (6 sides)		7.32E-2	5.31E-10	2.71	0.11 mBq/m^3	0.04 mBq/m^3	258 +/- 6%
C (CsI+Si)		2.40E-2	2.70E-07	2.71	0.61 mBq/m^3	0.22 mBq/m^3	45 +/- 15%
SAUNA					<0.2 mBq/m^3		
A (2 sides)	^{133}Xe	4.88E-3	1.05E-9	2.71	1.90 mBq/m^3	0.70 mBq/m^3	14 +/- 26%
B (6 sides)		7.32E-2	1.57E-8	2.71	0.13 mBq/m^3	0.05 mBq/m^3	214 +/- 7%
C (CsI+Si)		2.44E-2	1.02E-5	2.73	0.37 mBq/m^3	0.14 mBq/m^3	73 +/- 12%
SAUNA					0.18 mBq/m^3		
A (2 sides)	^{133m}Xe	4.96E-3	3.31E-11	2.71	1.54 mBq/m^3	0.57 mBq/m^3	18 +/- 24%
B (6 sides)		7.44E-2	4.96E-10	2.71	0.10 mBq/m^3	0.04 mBq/m^3	263 +/- 6%
C (CsI+Si)		2.48E-2	5.45E-09	2.71	0.56 mBq/m^3	0.21 mBq/m^3	48 +/- 14%
SAUNA					<0.2 mBq/m^3		
A (2 sides)	^{135}Xe	4.80E-3	2.49E-09	2.71	38 mBq/m^3	14 mBq/m^3	0.7 +/- 118%
B (6 sides)		7.20E-2	3.74E-08	2.71	2.53 mBq/m^3	0.94 mBq/m^3	11 +/- 31%
C (CsI+Si)		2.40E-2	2.44E-05	2.75	0.47 mBq/m^3	0.17 mBq/m^3	58 +/- 13%
SAUNA					<0.7 mBq/m^3		

The above computations show that detector geometries B and C can meet and exceed the MDC requirement in radioxenon monitoring stations of <1 mBq/m^3 for ^{133}Xe. A second station requirement, better than 15%–20% statistical precision for isotope ratios when present with more than 10 mBq/m^3, is met by the six-sided detector, except when ^{135}Xe is involved; the Si-CsI detector comes close. Optimized detector designs, possibly with secondary CsI, CdTe, or CZT detectors, should be able to improve the MDC and statistics.

The detection limit n_{LD} is dominated by the term 2.71 since the coincidence background counts in the ROI are in the order of 10^{-5} or less. If the coincidence requirement would be omitted (e.g., looking only at ROIs for 30 keV X-rays or 129 keV CEs), n_{LD} will be in the order of 10^1 to 10^2; thus, background would contribute noticeably and worsen the MDC.

We note that in some applications, MDC may not be the most appropriate measure of sensitivity. For example, in on-site inspections, a large number of samples have to be tested, and one can imagine a two-stage procedure: first, testing samples to learn if they contain radioxenon at all and second, measuring more closely those that do. The first test then needs to determine only if it is likely that radioxenon is present. This is true if the total count in the ROIs is greater than L_C. Since L_C for Si detectors is in the order or 10^{-5} or less, in principle, a single count in the coincidence ROIs indicates that radioxenon is present. In such applications, L_C is thus the more appropriate measure, and Si detectors far exceed the existing detectors where – estimated from published MDC – L_C is in the order of 10^2. A few hours of counting per sample may be sufficient to separate samples that are likely to contain radioxenon from those that are undetermined.

CONCLUSIONS AND RECOMMENDATIONS

In summary, we performed radiation transport simulations and measurements with test sources to characterize Si detectors for radioxenon measurements. For simulated electrons, the probability to deposit full energy in one 100 mm^2 side of a Si detector is about 12% (i.e., 72% in a six-sided Si detector cube). For photons, the full energy deposition probability depends strongly on the energy, ranging from 14.4% at 4.1 keV to 2.0% at 30 keV and ≤ 0.1% for 80 keV and higher (for each side). Using a variety of solid and gas sources, we measured detector backgrounds and energy resolutions at key energies with SDD and PIN detectors, e.g., at 30 keV, ~300 eV FWHM cooled, and ~420-600 eV FWHM RT for a small PIN. This means the cheaper PIN diodes can be used, ideally without the complexity of cooling, and still achieve the key requirement of separating the 30/31 keV X-rays from different radioxenon isotopes. The results from simulations and measurements were used to estimate the MDC of radioxenon isotopes in a variety of detector configurations. We found MDCs of 1.5–1.9 mBq/m^3 for most isotopes with a simple 1 cm^3 cube detector with two active sides and around 0.1 mBq/m^3 for a cube with six active sides. The exception is ^{135}Xe, for which the MDC is ~38 mBq/m^3 with the two-sided cube and ~2.5 mBq/m^3 with the six-sided cube. Addition of a CsI detector element improves the ^{135}Xe MDC to below 1 mBq/m^3 and increases counts to improve statistical errors.

Si detectors thus meet several key requirements for detectors in radioxenon monitoring stations. With their lower complexity and ability to detect ^{37}Ar L X-rays in the same detector, they are also a good match for on-site inspection applications, especially for fast screening. Discussions with Si detector manufacturers concluded that there are no fundamental obstacles to building Si detector cubes, although obtaining large detectors at a reasonable cost is a concern.

ACKNOWLEDGEMENTS

We greatly appreciate the help of S. Biegalski and T. Tipping, who accommodated us at short notice for Xe measurements at the University of Texas at Austin.

REFERENCES

Anderson, A. and A. Ringbom (2003). Xenon air activity concentration analysis from coincidence data, FOI report 0913 (FOI-R--0913--SE).

Browne, E. and R. Firestone (1986). *Table of Radioactive Isotopes*, J. Wiley.

Currie, L. A. (1968). Limits for qualitative detection and quantitative determination: Application to radiochemistry, *Anal. Chem.* 40: 586–593.

Fontaine, J-P., F. Pointurier, X. Blanchard, and T. Taffary (2004). Atmospheric xenon radioactive isotope monitoring, *J. Environ. Radioact.* 72: 129.

Gatti, E. and P. Rehak (1984). Silicon drift detector; studies about geometry of electrodes and production technology, *Nucl. Instrum. Methods Phys. Res., Sect. A* 225: 608.

Gohla, H. and M. Auer (2010). 1st IMS noble gas system certification—Review of certification requirements, *Proceedings of 2010 INGE Workshop* (day 2, session 5).

Goulon, J., A. Rogalev, G. Goujon, C. Gauthier, E. Moguiline, A. Solé, S. Feite, F. Wilhelm, N. Jaouen, C. Goulon-Ginet, P. Dressler, P. Rohr, M.-O. Lampert, and R. Henck (2005). Advanced detection systems for X-ray fluorescence excitation spectroscopy, *J. Synchrotron Radiation* 12: 57.

Hennig, W., H. Tan, A. Fallu-Labruyere, W. K. Warburton, J. I. McIntyre, and A. Gleyzer (2007). Characterization of phoswich well detectors for radioxenon monitoring, in *Proceedings of the 29th Monitoring Research Review: Ground-Based Nuclear Explosion Monitoring Technologies*, LA-UR-07-5613, Vol. II, pp. 757–763.

Hennig, W., W. K. Warburton, A. Fallu-Labruyere, K. Sabourov, M. W. Cooper, J. I. McIntyre, A. Gleyzer, M. Bean, E. P. Korpach, K. Ungar, W. Zhang, and P. Mekarski (2009). Development of phoswich detector system for radioxenon monitoring, *J. Radioanal. Nucl. Chem.* 282: 681.

Ringbom, A., T. Larson, A. Axelson, K. Elmgren, and C. Johansson (2003). SAUNA—A system for automatic sampling, processing and analysis of radioactive xenon, *Nucl. Instrum. Methods Phys. Res., Sect. A* 508: 542–553.